GEOPHYSICAL RESEARCH LETTERS, VOL. 36, L10203, doi:10.1029/2008GL037108, 2009

Electron density dropout near Enceladus in the context of water-vapor and water-ice

W. M. Farrell,[1] W. S. Kurth,[2] D. A. Gurnett,[2] R. E. Johnson,[3] M. L. Kaiser,[1] J.-E. Wahlund,[4] and J. H. Waite Jr.[5]

Received 22 December 2008; revised 26 March 2009; accepted 1 April 2009; published 20 May 2009.

[1] On 12 March 2008, the Cassini spacecraft made a close encounter with the Saturnian moon Enceladus, passing within 52 km of the moon. The spacecraft trajectory was intentionally-oriented in a southerly direction to create a close alignment with the intense water-dominated plumes emitted from the south polar region. During the passage, the Cassini Radio and Plasma Wave System (RPWS) detected two distinct radio signatures: 1) Impulses associated with small water-ice dust grain impacts and 2) an upper hybrid (UH) resonance emission that both intensified and displayed a sharp frequency decrease in the near-vicinity of the moon. The frequency decrease of the UH emission is associated with an unexpectedly sharp decrease in electron density from ~90 el/cm^3 to below 20 el/cm^3 that occurs on a time scale of a minute near the closest encounter with the moon. In this work, we consider a number of scenarios to explain this sharp electron dropout, but surmise that electron absorption by ice grains is the most likely process.
Citation: Farrell, W. M., W. S. Kurth, D. A. Gurnett, R. E. Johnson, M. L. Kaiser, J.-E. Wahlund, and J. H. Waite Jr. (2009), Electron density dropout near Enceladus in the context of water-vapor and water-ice, *Geophys. Res. Lett.*, *36*, L10203, doi:10.1029/2008GL037108.

1. Introduction

[2] A major discovery of the Cassini mission was the observation of a substantial water geyser at the south pole of Saturn's moon Enceladus [*Porco et al.*, 2006; *Waite et al.*, 2006; *Hansen et al.*, 2006]. The emitted water 1) is believed to be the source of the large toroidal cloud of hydroxyl radicals with a peak density near 4 R_s previously observed by HST [*Shemansky et al.*, 1993], 2) creates an extended neutral and plasma torus that drives processes in the inner magnetosphere [*Richardson and Jurac*, 2004; *Jurac and Richardson*, 2005, 2007], and 3) is the source of ice comprising the E-ring [*Haff et al.*, 1983; *Horányi et al.*, 2008]. The observation of both water and internal energetic activity at the moon places Enceladus on a growing list of astrobiological targets-of-interest that includes Titan, Mars, Europa, comets, and asteroids.

[3] Given this extraordinary find, the Cassini science operations team planned a set of close spacecraft passages by the moon to obtain further details of its structure and physical processes. One such encounter occurred on 12 March 2008. Figure 1 shows the trajectory of the spacecraft in an Enceladus frame of reference where +x is oriented in the direction of the moon's orbital velocity, +y is oriented towards Saturn, and +z is oriented out of the moon's orbital plane. The water plume is illustrated in Figure 1 as the purple-shaded region approximately indicating the location of highest water density. The spacecraft moved primarily southward at ~14 km/sec, passing near and aligned with the water geysers. Given that Enceladus' radius is ~250 km, the entire encounter (defined herein as ± 5 radii about the moon) lasted for a little over 4 minutes, and the encounter with peak geyser activity itself transpired on a timescale of minutes.

[4] The Cassini Ion and Neutral Mass Spectrometer (INMS) [*Waite et al.*, 2004] found (on a previous encounter) that the geysers consisted of emissions similar in nature to cometary plumes – a dominance of water molecules but also the presence of methane, carbon monoxide, carbon dioxide, and both simple and complex organics [*Waite et al.*, 2006]. During this 12 March 2008 encounter, the INMS-measured water concentration was found to be <10^4/cm^3 before closest approach (CA) at 19:06:11 SCET, outside the plume. However, concentrations increased sharply thereafter peaking near 10^7/cm^3 between ~19:06:30–19:07:00 SCET. During this period, the spacecraft was traveling aligned with the plume but also migrating axially-inward toward the gas center- intersecting its largest concentrations at approximately 300 km from the southerly-directed surface source. Passing southerly at larger radial distances, INMS continued to detect plume emissions at levels > 3 × 10^5/cm^3 as late at 600 seconds after CA.

[5] As we demonstrate herein, the presence of large concentrations of water changes the very nature of the plasma-neutral interactions. Specifically, prior to CA, the plasma can be considered collisionless. In contrast, during the close encounter, the plasma electrons have many collisions with water vapor and ice such that its effect on the plasma inflow cannot be immediately neglected. The effect is to create a steady depletion of electrons with inward radial distance that is reminiscent of the exponential electron decrease at the bottom-side of an ionosphere – but now defined by water gas and ice chemistry.

2. Observations

[6] Figure 2 shows a Cassini Radio and Plasma Wave Science (RPWS) radio spectrogram [*Gurnett et al.*, 2004]

[1]Space Exploration Directorate, NASA Goddard Space Flight Center, Greenbelt, Maryland, USA.
[2]Department of Physics and Astronomy, University of Iowa, Iowa City, Iowa, USA.
[3]Department of Material Science and Engineering, University of Virginia, Charlottesville,Virginia, USA.
[4]Swedish Institute of Space Physics, Uppsala, Sweden.
[5]Space Science and Engineering, Southwest Research Institute, San Antonio, Texas, USA.

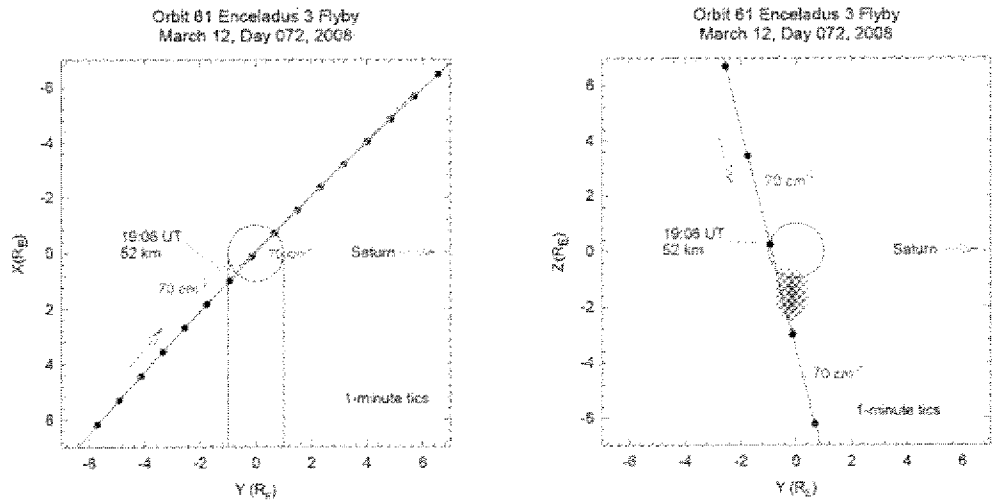

Figure 1. The trajectory of the Cassini spacecraft past Enceladus, with (left) showing a 'top' view looking down from above the orbital plane and (right) showing meridional view looking opposite the direction of the orbital velocity vector. The electron concentration drops below 70 cm^{-3} between the red markers.

encompassing a 30 minute period centered about the Enceladus encounter. Closest approach to the moon (52 km above the surface) is indicated in Figure 2. The measurements are from the wideband waveform system with a 3-dB bandwidth of ~75 kHz. The upper hybrid emission (f_{uh}) and electron cyclotron frequency (f_{ce} - derived from magnetometer results) are presented on Figure 2 for reference.

[7] In this presentation, there are two clear and distinct signals: 1) A broadband signal (bandwidth of ~80 kHz) that commences near 18:55 SCET and extends to at least 19:20 SCET that consist of impulsive spike-like events resulting from micron-sized dust grain impacts on the spacecraft system [*Gurnett et al.*, 1983; *Kurth et al.*, 2006; *Wang et al.*, 2006] and 2) and upper hybrid emission (labeled f_{uh} in the spectrogram) that displays a clear and distinct frequency downshift centered about CA. Unfortunately, the intense broadband dust impact signatures obscure the upper hybrid emission between 19:06 to 19:07:30 SCET when the impact rate is highest, making it difficult to track the band throughout the entire interval. However, a period of emission frequency down-shift is observed between 19:05–19:06 SCET and up-shift to near pre-encounter levels between 19:07:30–19:08 SCET.

[8] Regarding (1), water-ice dust grains are incident on the spacecraft and antenna, creating impact ionizations that are detected as a bipolar voltage pulse on time scales of a few milliseconds [*Gurnett et al.*, 1983]. When Fourier-transformed into a frequency-versus-time spectrogram they

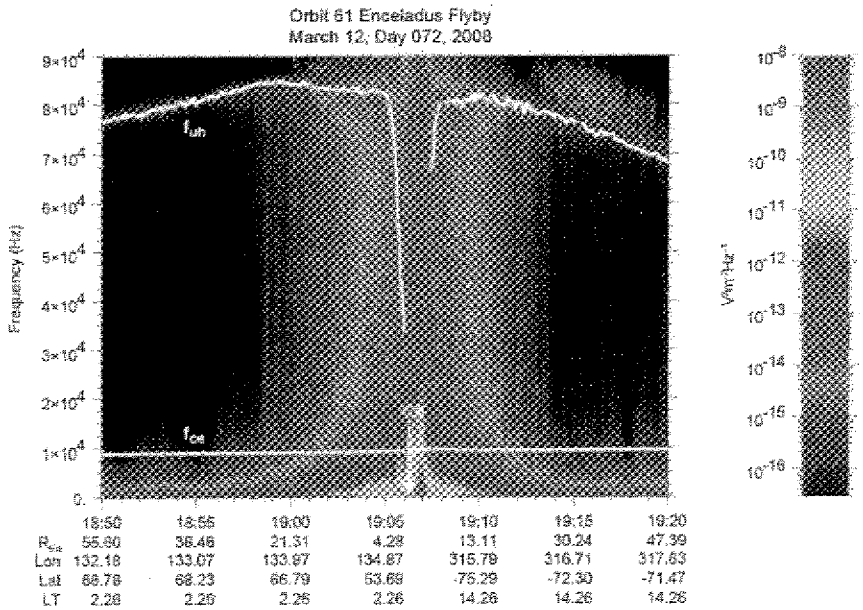

Figure 2. Cassini RPWS wideband waveform spectrograms showing both the broadband impulsive dust grain impacts and upper hybrid emission (f_{uh}). The electron cyclotron frequency is also indicated for reference. Closest approach to the moon is indicated by CA.

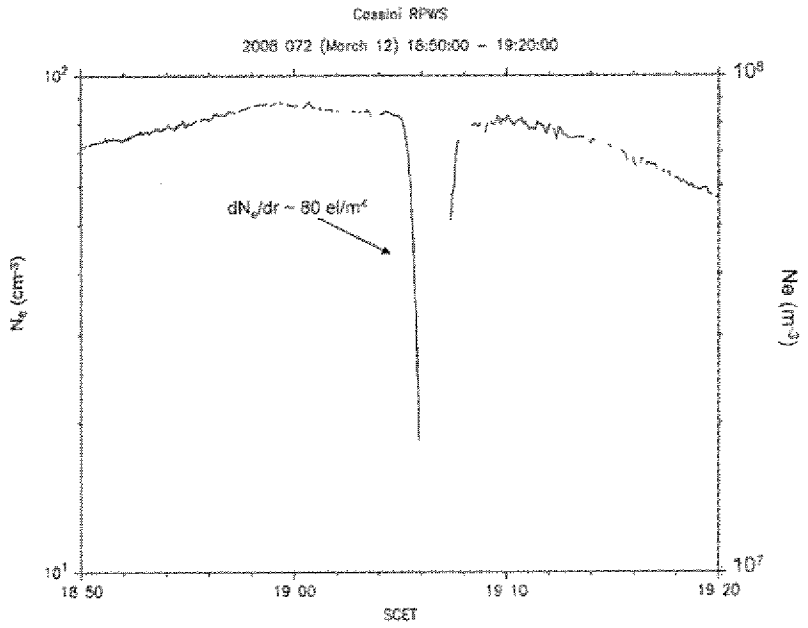

Figure 3. The electron density (in cm^{-3} and m^{-3}) as derived from the upper hybrid resonance emission.

form a broadband impulsive event extending to the limit of receiver bandwidth. A clearly-presented derivation of the dust charge transfer transform is provided in the appendix of *Wang et al.* [2006]. During the Enceladus encounter, dust grain impact rates progressively increased from 18:56 SCET, peaking on the order of 1000/sec between 19:04–19:10 SCET. Impact rates progressively decreased thereafter. During peak activity near CA, the bandwidths were observed to increase to large extents. The impact rate appears to have an abrupt decrease near 19:14 SCET, but still some level of impact detection persists intermittently to beyond 19:20 SCET.

[9] Regarding (2), an upper hybrid emission is typically detected throughout the entire inner magnetosphere [*Gurnett et al.*, 2005; *Persoon et al.*, 2005, 2006]. It allows a derivation of the electron plasma frequency (since $f_{pe} = (f_{uh}^2 - f_{ce}^2)^{1/2}$) and thus electron density at a planet-centered radial distance of 2–10 Saturn radii. Well away from the moon, the upper hybrid emission (i.e., the electron density) varies in a progressive fashion, with variations on scale sizes of a fraction of a Saturn radii [see *Persoon et al.*, 2006, Figure 5]. However, Figure 2 indicates that very near Enceladus, there is a significant reduction in f_{uh} indicating the presence of a clear and distinct 'bite-out' in electron density that was not anticipated – occurring on spatial scales of a few Enceladus radii. In fact, due to pick-up processes [*Tokar et al.*, 2006; *Pontius and Hill*, 2006] the plasma flow velocity near Enceladus has been measured to slow substantially from ~26 km/sec to <10 km/sec [*Wahlund et al.*, 2005, 2008]. The plasma densities would thus be expected to increase by a factor of 2–3 in the near-vicinity of the moon in order to conserve flux. Clearly, such an increase is not observed for electrons and an unexpected, sharp decrease was observed instead.

[10] Figure 3 shows the derived electron density from the f_{uh} emission which displays the clear and distinct dropout in electron density. Note that between 19:05 and 19:06 SCET, the electron density decrease with radial distance from Enceladus, dn_e/dr, is on the order of -80 el/m^4. This large negative gradient can be considered a primary marker that defines the values of the source and loss terms in the electron continuity equation. By the time Cassini exits the plume, the electron density has recovered to approximately its pre-encounter level.

3. Interpretation

[11] The electron continuity equation can be written as $\partial n_e/\partial t + \nabla \cdot (n_e \mathbf{v}_e) = S - L$ where $\mathbf{v}_e$ is the electron flow speed past the moon, S are electron sources (primarily photo-ionization) and L are electron loss processes that include electron recombination, electron dissociative attachment and a new term defining dust absorption.

[12] Assuming a time-stationary situation (constant gas emission and steady spatial gradient) then $\partial n_e/\partial t = 0$. One can write an approximate 1-D electron continuity equation along the Cassini trajectory past the moon as:

$$\begin{aligned} \partial(n_e v_e)/\partial s &= v_e \partial n_e/\partial s + n_e \partial v_e/\partial s \\ &= \nu n_{H2O} - k_r n_e^2 - k_d n_{H2O} n_e - \eta_d v_e n_e \end{aligned} \quad (1)$$

where the left hand side describes the divergence of the electron flux upon approach to the moon, and the right hand side accounts for sources and losses with a water photo-ionization source described by $\nu\ n_{H2O}$, electron recombination losses with water ions (of assumed comparable density as electrons) described as $\sim k_r n_e^2$, electron dissociative attachment losses described by $k_d\ n_{H2O}\ n_e$, and electron losses via dust absorption defined as $\eta_d\ v_e\ n_e$ [*Jackson et al.*, 2008].

[13] We will now apply this equation during the period before CA between 19:05–19:06 SCET, during the RPWS-observed very steep electron density gradient of $\partial n_e/\partial s \sim -80$ el/m^4. The electron density, n_e, was $\sim 8 \times 10^7$/m^3 at

the start of the drop-out period near 19:05 SCET and $<2 \times 10^7/m^3$ at the end of the period near 19:06 SCET (the band is difficult to identify between 19:06–19:07:30 SCET). We note that during this period, n_{H2O} was not at its peak levels, but ranges from $0.2–1.0 \times 10^{10}/m^3$.

[14] Regarding the flux divergence during this time, both electron density and velocity are undergoing changes upon approach to the moon. Specifically, due to pickup/mass loading effects, the plasma flow speed was previously observed to progressively slow from corotational values of 26 km/sec at ~14 R_e to below 10 km/sec at 9 R_e [*Tokar et al.*, 2006; *Wahlund et al.*, 2005; *Pontius and Hill*, 2006; *Wahlund et al.*, 2008]. Close to the moon, the flows should slow substantially (in theory, approaching zero). The previously-observed plasma flow measurements suggest a velocity gradient that decreases with approach to the moon as $\partial v_e/\partial s \sim -0.007/s$. If there were no other sources or losses, the electron density gradient should become positive to keep the flux constant in the progressively slower flow. However, we instead observe a strongly decreasing electron density with inward distance, and conclude there must be a very substantial loss mechanism.

[15] Assuming that the decrease in flow speed described above continues into the plume, the flow speed would then become $v_e \sim 7$ km/s near 4.3 R_e. Using $n_e \sim 8 \times 10^7/m^3$, the divergence of the flux $\partial(n_e v_e)/\partial s \sim -10^6$ el/m^3-s. The loss processes described on the right hand side of the continuity equation (1) must then account for this rate on the left hand side of the equation.

[16] The first term on the right-hand side of equation (1) represents the photoionization sources of electrons. The photoionization rate of H_2O, ν, at Saturn is $\sim 4 \times 10^{-9}$/sec [*Richardson et al.*, 1998] and for Cassini INMS-measured water levels at $\sim 10^{10}/m^3$, we obtain a small source term, S, of +40 el/m^3-s.

[17] Electron dissociative recombination ($H_2O^+ + e = H + OH$) is considered the dominant recombination process [*Richardson*, 1992] and the process that appears to limit the molecular ion life time near the orbit of Enceladus [*Sittler et al.*, 2008]. The recombination rate constant, k_r, was calculated using the integral $k_r = (2e/m)^{1/2} \int \sigma_r(u)\, u\, f(u)\, du$, where u is the energy in eV, and $\sigma_r(u)$ the cross-section of *Mul et al.* [1983] varying approximately as $\sim u^{-3/2}$. We assume a Maxwellian distribution of electrons with thermal energy u_e, $f(u) = 2\pi^{-1/2} u_e^{-3/2} \exp(-u/u_e)$, such that $\int u^{1/2} f(u)\, du = 1$. We find that $k_r \sim 7 \times 10^{-15}$ m^3/s assuming a 5 eV electron temperature. In a quasi-neutral situation, $n_{H2O+} \sim n_e$, and the losses from electron dissociative recombination, $-k_r n_e^2$, are −45 el/m^3-s (as we discuss below, the plasma is most likely neutral to order of magnitude). As such, recombination appears to just offset photo-ionization sources during this period.

[18] Losses via electron dissociative attachment can also be derived. Near 6.5 eV, an electron can dissociate water predominately into OH and H- ($e + H_2O = OH + H^-$). The cross section for this process has a peak near 5×10^{-22} m^2 and a width of $\Delta u \sim 1$ eV [*Itakawa and Mason*, 2002; *Delory et al.*, 2006]. The rate constant is thus $k_d \sim (2e/m)^{0.5} \sigma_d(u_d)\, u_d\, f(u_d)\, \Delta u \sim 5 \times 10^{-17}$ m^3/s, with $u_d = 6.5$ eV and $u_{th} = 5$ eV. The loss rate for this process is thus $-k_d n_{H2O} n_e \sim -40$ el/m^3-s, a relatively small value as well.

[19] Herein then lies our dilemma: If we consider the usual processes associated with water molecules - photoionization, recombination, and dissociation - along the Cassini transit, we find that none of these molecular source and loss processes at ~ a few 10's of el/m^3-s can account for the intense electron flux divergence at -10^6 el/m^3-s. These water molecules and ion processes alone cannot account for the severe loss of electrons observed before CA.

[20] However, as indicated in Figure 2, there is clearly the presence of water-ice (dust) in the environment and this also can alter the plasma character. In equation (1), the effect of this dust absorption is quantified via the $-\eta_d v_e n_e$ term, where $\eta_d = \sigma_d n_d$ is the inverse of the dust/electron collision mean free path [*Jackson et al.*, 2008]. The quantity n_d is the dust density and σ_d is the dust/electron collision cross-section, πa_{eff}^2, where a_{eff} is an 'effective capture radius' about the dust grain.

[21] We now consider the constraints on dust particulate absorption of electrons that are required to be consistent with the divergence of the flux (left hand side of equation (1)) – in essence reversing the argument to examine self-consistency. If we assume that the observed flux divergence is created solely and completely by dust absorption, and define electron flux as $g = n_e v_e$ we find that $dg/ds \sim -10^6$ el/m^3-s, $= -\eta_d g$. For $n_e = 8 \times 10^7/m^3$ and $v_e = 7$ km/sec, we find that $\eta_d = g^{-1}\, dg/ds \sim 10^{-6}$/m. Given that η_d is also equal to $\sigma_d n_d$, we now want to get an independent estimates of dust density, n_d, to determine if the self-consistent dust cross section is in any way realistic for this value of η_d.

[22] As indicated in Figure 2, during the Cassini Enceladus flyby, dust (water-ice) was directly detected via impact ionization in an extended region about the body (±30 R_e) symmetric about CA. Based on counting RPWS wideband waveform bipolar impact signatures, it was found impacts on the approximate order of 1000 per second were detected between 19:04–19:10 SCET. So many impacts occurred during this period that the automated counter run in the RPWS ground data processing system saturated. The incident dust flux (#/second) being sensed by RPWS is $F = n_d v A > 1000$/second. For a spacecraft speed of ~14 km/sec and effective spacecraft collecting area of ~0.4 m^2 [*Kurth et al.*, 2006; *Wang et al.*, 2006], this count rate translates to a dust density exceeding $n_d > 0.2/m^3$.

[23] Given the constraint on η_d and an independent impact-based estimate of n_d, we find an effective cross-section for the electron absorbers to be $\sigma_d = \eta_d/n_d < 5 \times 10^{-6}$ m^2 which corresponds to a predicted effective radius of less than about 1 millimeter – consistent with electron absorption by small particles. Thus, the observed changes in electron flux can be considered consistent with the presence of large concentrations ($> 0.2/m^3$) of small absorbers (<1 mm). We note that these are bounding values and there may be larger concentrations of substantially smaller submicron sized grains that would go undetected via impact ionization with the RPWS antenna system [*Kurth et al.*, 2006]. The formalism also applies to water clusters (groups of molecules) that may be large in number and also absorbing electrons (although the process may be more similar to dissociative attachment at the cluster level).

[24] In the above argument, the detailed electrostatic processes are effectively 'lumped' into the absorption cross

section, σ_d, which provides limited physical insight. We now consider an independent dust-plasma electrostatic model by *Goertz* [1989] that describes the micro-physical interaction between the plasma and dust. The model indicates that the electrostatic nature of the dusty-plasma is quantified by a P-factor defined as (a u_e) (n_d/n_e), where a is the grain radius and u_e is the electron plasma temperature in eV [see *Goertz*, 1989, Figure 5, Table 1]. For $P > 10^{-12}$ m-eV, the larger concentration of grains creates overlapping Debye sheaths that leaves the inter-grain gas medium with an overall negative plasma potential [see *Goetz*, 1989, Figure 4]. Applying the limits provided by the continuity equation (i.e., $a_{eff} \sim 10^{-3}$ m, $n_d \sim 0.2/m^3$, $u_e \sim 5$ eV, and $n_e \sim 8 \times 10^7$ m^3) we find that $P \sim 10^{-11}$ m-eV and conclude that the dusty-plasma should indeed be acting in a collective way. From *Goertz* [1989, Figure 5] at $P \sim 10^{-11}$ m-eV, the plasma potential drop is predicted to be $\phi \sim -0.7\ kT_e/e$ or a few volts negative, and should result in (at least) a factor of 2 decrease in electron density. In fact, the RPWS Langmuir Probe detected a clear and distinct drop in plasma potential of a few volts exactly coincident with the near-Enceladus electron dropout.

4. Conclusions

[25] We considered a number of possible loss processes to explain the near-Enceladus electron drop-out including water-ion recombination and water molecule dissociation, but found that these could not generate the sharp and distinct gradient. However, if we consider absorption of electrons via water-ice of sub-millimeter scale size, we find that indeed the observed water-ice concentrations are large enough to account for the electron depletion and associated plasma potential drop both measured by Cassini.

References

Delory, G. T., et al. (2006), Oxidant enhancement in Martian dust devils and storms: Storm electric fields and electron dissociative attachment, *Astrobiology, 6*, 451.

Goertz, C. K. (1989), Dusty plasmas in the solar system, *Rev. Geophys., 27*, 271.

Gurnett, D. A., et al. (1983), Micron-sized particles detected near Saturn by the Voyager plasma wave instrument, *Icarus, 53*, 236.

Gurnett, D. A., et al. (2004), The Cassini radio and plasma wave investigation, *Space Sci. Rev., 114*, 395.

Gurnett, D. A., et al. (2005), Cassini radio and plasma wave observations near Saturn, *Science, 307*, 1255.

Haff, P. K., et al. (1983), Ring and plasma: The enigma of Enceladus, *Icarus, 56*, 426.

Hansen, C. J., et al. (2006), Enceladus' water vapor plume, *Science, 311*, 1422.

Horányi, M., A. Juhász, and G. E. Morfill (2008), Large-scale structure of Saturn's E-ring, *Geophys. Res. Lett., 35*, L04203, doi:10.1029/2007GL032726.

Itakawa, Y., and N. Mason (2002), Cross sections for electron collisions with water molecules, *J. Phys. Chem. Ref. Data, 34*, 1.

Jackson, T. L., W. M. Farrell, G. T. Delory, and J. Nithianandam (2008), Effect of dust absorption on the electron avalanche process occurring within Martian dust storms, *Geophys. Res. Lett., 35*, L16201, doi:10.1029/2008GL034523.

Jurac, S., and J. D. Richardson (2005), A self-consistent model of plasma and neutrals at Saturn: Neutral cloud morphology, *J. Geophys. Res., 110*, A09220, doi:10.1029/2004JA010635.

Jurac, S., and J. D. Richardson (2007), Neutral cloud interaction with Saturn's main rings, *Geophys. Res. Lett., 34*, L08102, doi:10.1029/2007GL029567.

Kurth, W. S., et al. (2006), Cassini RPWS observations of dust in Saturn's E ring, *Planet. Space Sci., 54*, 988.

Mul, P. M., et al. (1983), Merged electron-ion beam experiments: V. Dissociative recombination of OH^+, H_2O^+, H_3O^+ and D_3O^+, *J. Phys. B At. Mol. Phys., 16*, 3099.

Persoon, A. M., D. A. Gurnett, W. S. Kurth, G. B. Hospodarsky, J. B. Groene, P. Canu, and M. K. Dougherty (2005), Equatorial electron density measurements in Saturn's inner magnetosphere, *Geophys. Res. Lett., 32*, L23105, doi:10.1029/2005GL024294.

Persoon, A. M., D. A. Gurnett, W. S. Kurth, and J. B. Groene (2006), A simple scale height model of the electron density in Saturn's plasma disk, *Geophys. Res. Lett., 33*, L18106, doi:10.1029/2006GL027090.

Pontius, D. H., Jr., and T. W. Hill (2006), Enceladus: A significant plasma source for Saturn's magnetosphere, *J. Geophys. Res., 111*, A09214, doi:10.1029/2006JA011674.

Porco, C. C., et al. (2006), Cassini observes the active south pole of Enceladus, *Science, 311*, 1393.

Richardson, J. D. (1992), A new model for plasma transport and chemistry at Saturn, *J. Geophys. Res., 97*, 13,705.

Richardson, J. D., and S. Jurac (2004), A self-consistent model of plasma and neutrals at Saturn: The ion tori, *Geophys. Res. Lett., 31*, L24803, doi:10.1029/2004GL020959.

Richardson, J. D., et al. (1998), OH in Saturn's magnetosphere: Observations and implications, *J. Geophys. Res., 103*, 20,245.

Shemansky, D. E., et al. (1993), Detection of the hydroxyl radical in Saturn's magnetosphere, *Nature, 363*, 329.

Sittler, E. C., et al. (2008), Ion and neutral sources and sinks within Saturn's inner magnetosphere: Cassini results, *Planet. Space Sci., 56*, 3.

Tokar, R. L., et al. (2006), The interaction of the atmosphere of Enceladus with Saturn's plasma, *Science, 311*, 1409.

Wahlund, J.-E., et al. (2005), The inner magnetosphere of Saturn: Cassini RPWS cold plasma results from the first encounter, *Geophys. Res. Lett., 32*, L20S09, doi:10.1029/2005GL022699.

Wahlund, J.-E., et al. (2008), Detection of dusty plasma near the E-ring of Saturn, *Planet. Space Sci.*, in press.

Waite, J. H., Jr., et al. (2004), The Cassini ion and neutral mass spectrometer (INMS) investigation, *Space Sci. Rev., 114*, 113.

Waite, J. H., Jr., et al. (2006), Cassini ion and neutral mass spectrometer: Enceladus plume composition and structure, *Science, 311*, 1419.

Wang, Z., et al. (2006), Characteristics of dust particles detected near Saturn's ring plane with the Cassini radio and plasma wave instrument, *Planet. Space Sci., 54*, 957.

W. M. Farrell and M. L. Kaiser, Space Exploration Directorate, NASA Goddard Space Flight Center, Code 695, Greenbelt, MD 20771, USA. (william.farrell@gsfc.nasa.gov)

D. A. Gurnett and W. S. Kurth, Department of Physics and Astronomy, University of Iowa, 715 Van Allen Hall, Iowa City, IA 52242, USA.

R. E. Johnson, Department of Material Science and Engineering, University of Virginia, Charlottesville, VA 22903, USA.

J.-E. Wahlund, Swedish Institute of Space Physics, PO Box 537, SE-751 21 Uppsala, Sweden.

J. H. Waite Jr., Space Science and Engineering, Southwest Research Institute, 6220 Culebra Road, San Antonio, TX 78238-5166, USA.